JOURNAL OF AEROSPACE SOCIETY MALAYSIA

ARTICLE

COMPUTATIONAL AERODYNAMICS ANALYSIS OF A BLUFF BODY WITH ROTATING CYLINDER AS DRAG REDUCER

Muhammad Irfan Kamid [1], Hidayatullah Mohammad Ali [1,*] and Azmin Shakrine Mohd Rafie [1]

1. Department of Aerospace Engineering, Faculty of Engineering, Universiti Putra Malaysia, 43400 Serdang, Selangor, Malaysia

*Correspondence: hidayatmaddali@gmail.com

Abstract: This study is aimed to address the issue of dangerous emissions into the environment by the operation of large container lorries. These big vehicles use much of their engine power to overcome the aerodynamic drag due to their movement, which also means a lot of fuel is being burned in this process. To reduce the fuel consumption, hence the gas emissions, the aerodynamic efficiency of the vehicle can be improved through its design. Based on this notion, the main objective of this work is to analyse the impacts from the use of a rotating cylinder as a drag reducer for heavy-duty vehicles. The incorporation of the rotating cylinder is expected to be able to reduce the drag forces acting on the vehicles and also increase their design aerodynamic efficiency. For this study, a container lorry is modelled and analysed using the computational simulation software, ANSYS with several different placements of the rotating cylinder around the lorry as its drag reducers. The obtained results indicate that the use of the cylinder can reduce drag by as much as 36% in comparison to the baseline design of the container lorry without rotating cylinder. It is observed that the cylinder helps to lessen the airflow circulating at the back and top of the container lorry, subsequently lower its drag coefficient. All in all, the findings from this study demonstrate the potential of using rotating cylinders as drag reducers to solve the issue of gas emissions from container lorries.

Keywords: ANSYS; aerodynamics analysis; bluff body; rotating cylinder; drag reducer

1. Introduction

Bluff bodies have been scientifically studied with regard to their aerodynamic characteristics and it is of particular interest to establish their drag performance with blunt bases. Designs of bluff bodies can be related to large road vehicles and their studies help to better understand the vehicles' aerodynamics. For instance, for a typical Class 8 line-haul tractor-trailer vehicle running at highway speeds, its resultant aerodynamic drag will cause considerable parasitic loss. In fact, a typical heavy truck vehicle uses around 65% of its entire energy at a speed of 70 mph to overcome aerodynamic drag [1]. Over the last decades, due in part by increase in fuel prices and also environmental concerns, researchers have made significant advancement in understanding the mechanisms for drag reduction with blunt-based bluff bodies [2]. In conjunction to this, aerodynamic performance has been considered in many road vehicle designs, which leads to mostly tapered design shapes to minimize the drag pressure. However, for heavy road vehicles such as container lorries, this entails significant design changes that could undesirably compromise their cargo capacity. Therefore, instead of changing the overall vehicle designs, it can be observed that some add-on features are applied to the existing heavy road vehicle designs to help improve their aerodynamic performance. In this case, aerodynamically-designed add-on parts are attached to the front as well as the other parts of the heavy road vehicle, which will adjust the effective form or shape of the vehicle to be more streamlined without altering its projected frontal area. Due to their exterior forms, sizes and also

positions, the external attachments can reduce the aerodynamic drag of the heavy road vehicles [3]. As a result, the reduced aerodynamic drag will improve the vehicle's fuel economy and lower its greenhouse gas emissions [4]–[7].

Thus far, the aerodynamic effects of many existing models of aerodynamic fairings (front and side) and their configurations have not been thoroughly researched or documented. Base drag is one of the key contributions to aerodynamic drag, which is the factor that determines fuel consumption. According to prior research, the base drag occurs in the back end of the vehicle. For the heavy road vehicles such as the container lorries, this is where the cargo area is located. A bluff body vehicle traveling at constant speed on a flat level road will spend up to 40% of its fuel energy to counteract its aerodynamic drag and 45% to overcome its rolling resistance, leaving just 15% to drive the gear and losses [8]. Several methods have been applied to improve the aerodynamics of the vehicles including passive and active flow control methods. From previous conducted study, 4% improvement has been achieved by curving the back of the vehicle, 3% improvement with nose cone and 7% improvement with chassis skirt [9]. Furthermore, for commercial vehicles, the coefficient of drag, C_d falls as the windshield attack angle is increased [9]. In the meantime, a device has been patented for vehicles as illustrated in Figure 1, which features resilient prongs along the rear edge of the vehicle body, extending beyond the edge in a flow-wise direction [10]. The function of this device is to improve the aerodynamic performance by reducing the drag caused by airflow over the vehicle's rear edge. Each prong is separated from the next, and flexible enough to deflect above and below the first plane defined by the vehicle's surface under the impact of the airflow over the vehicle at a certain speed. The prongs may have a composite structure or incorporate a vulcanized rubber substance, with uniform or tapering cross-section and radial corners. These prongs can be repositioned from a deployed position to a retracted position, either manually or by attaching the device to a rotating frame member that can be rotated between the two positions. On the other hand, conducted study on a 1/6 model truck and trailer has shown improved aerodynamics by 12.5% and 28% through installation of vertical and horizontal spoilers on the vehicle's front, respectively [11]. Moreover, other exemplary improvement methods include the use of redirector plates [12] and flow deflectors [13]. However, it can be deduced that most of these body alterations are rather substantial and therefore rather unsuitable for the current container lorry designs as their cargo capacity may need to be sacrificed.

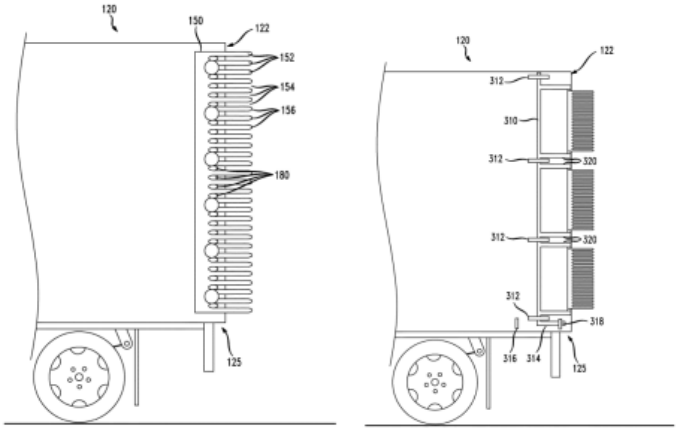

Figure 1: Aerodynamic drag reduction device [10]

Alternatively, it is believed that rotating cylinders have a good potential to be used as drag reducers for heavy road vehicles including container lorries. According to a conducted study, such devices could help to disrupt the airflow over and around the moving vehicle when they are installed on the front and back of the container or vehicle [14]. The rear spoiler is usually used to distribute the air, which lessens the turbulence that the moving vehicle creates, and subsequently aids in reducing air drag and turbulent

flow. On the other hand, a wind tunnel test for installation of rotating cylinder on a container lorry has been conducted and the obtained results indicate promising improvement in drag reduction [15]. Based on this notion, this study is aimed to investigate the aerodynamic effects from use of rotating cylinders as drag reducers for a container lorry that is considered as bluff body using computational fluid dynamics (CFD) method. The CFD simulation analysis in this study is done with ANSYS software tool.

2. Methodology

2.1. Pre-processing

ANSYS is a widely used CFD tool for simulating and analysing fluid flow and related phenomena. It utilises finite volume method (FVM) to discretise the governing equations, allowing for visualization and post-processing tasks. Known for its accuracy and user-friendliness, ANSYS is a widely applied tool for designing and optimising products and processes in various industries like aerospace, automotive, chemical and civil engineering. A mathematical model, consisting of equations and boundary conditions, is necessary for the numerical approach. FVM and *k*-epsilon model are used to solve the Navier-Stokes equations for two-dimensional Cartesian coordinates. The pre-processor, which essentially serves as the link between the user and the solver, provides a user-friendly interface and converts input for the solver.

For this study, the design of the 2D model of the container lorry is set with the dimension as listed in Table 1. In the previous conducted experimental work [15], the rotating cylinder is placed at the front of the container as indicated in Figure 2. The first placement of the cylinder is initially positioned at 215 mm as measured from the bottom of the container. On the other hand, the second and third considered placements of the cylinder are positioned at 16 mm and 32 mm below the first placement, respectively. As also illustrated in Figure 2, the computational analysis in this study also considers three new potential placements of the rotating cylinder at the back of the container. The first new placement is at the top back of the container. The second new considered placement is at the back rear corner of the container, which is 215 mm as measured from the bottom of the container. Last but not least, the third positioning of the rotating cylinder is at the rear top of the container, which is 50 mm higher than the new second positioning and 50 mm aft at the same height of the first new position.

As for the computational domain, a fluid volume of air has been created surrounding the vehicle in order to simulate the air movement around it. It should be noted that the dimensions of the domain are set to 3 m × 1.5 m (length × height) to match the average size of the wind tunnel used in the previous experimental setup. This will enable a direct validation study to be conducted through the comparison of results from the CFD simulation and the previous experimental work for the three initial positioning considered for the rotating cylinders on the container lorry. Figure 3 depicts the geometric modeling of the container lorry (clean design without the rotating cylinder) and the domain after their construction.

Table 1: Parameters of the container lorry model

Parameter	Value
Container's Height	0.240 m
Trailer's Height	0.180 m
Total Length	0.890 m
Container's Length	0.600 m
Trailer's Length	0.200 m
Cylinder's Radius	0.022 m

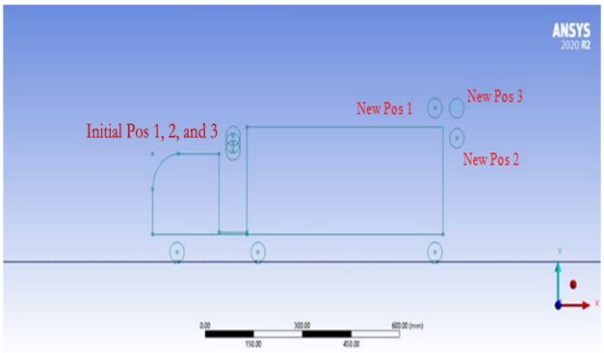

Figure 2: Illustration of the container lorry with considered positioning of rotating cylinder

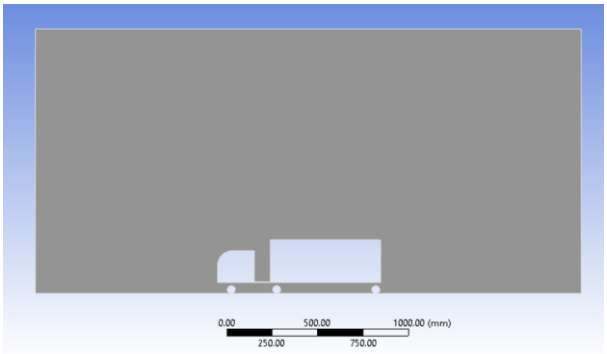

Figure 3: Computational analysis model of the container lorry with no rotating cylinder

Furthermore, grid generation is a crucial part of the CFD simulation process since it influences not only the simulation duration but also the accuracy of the results. In short, this refers to the creation of a mesh or grid that is associated with a domain and its boundaries. Edge sizing is used for the setting of the model where all of the meshes use 200 divisions on every edge. To achieve satisfactory results, it is recommended that the inflation parameters of a maximum of 10 layers and a growth rate of 1.2 are set on the surfaces of each model [16]-[18]. It should be noted that it has been discovered that the accuracy of computational results can be improved by using a small number of mesh elements [19]. The inflation layer is one of the important factors that affect the accuracy of CFD simulations. If the number of layers is insufficient, the simulation results will not be accurate. Meanwhile, when it is too large, the simulation time will increase. This supports the importance of selecting appropriate inflation parameters to achieve satisfactory CFD simulation results.

The detailed information on mesh settings and boundary conditions for this study are tabulated in Table 2 and the generated grid around the container lorry model is illustrated in Figure 4. As observed in Figure 4, named selection setting is used to name every boundary: inlet as 'velocity-inlet' ranging from 0 m/s to 32 m/s, road as 'ground', top wall as 'symmetry', whole container lorry as 'body', cylinder as 'cylinder' with 'no slip' condition and 'rotational' moving wall, and the outlet as 'pressure-outlet' where its pressure is set to constant and equals to the atmospheric pressure.

Table 2: The mesh setting for this study

Mesh Specification	
Growth Rate	1.2
De-feature Size	3.5e-004 m
Curvature Minimum Size	7.0e-004 m
Curvature Normal Angle	18.0 °
Smoothing	High
Skewness	0.18227
Orthogonal Quality	0.95941
Inflation Specification	
Smoothing	High
Inflation Option	First Layer Thickness
First Layer Height	0.1 mm
Maximum Layers	10
Growth Rate	1.2

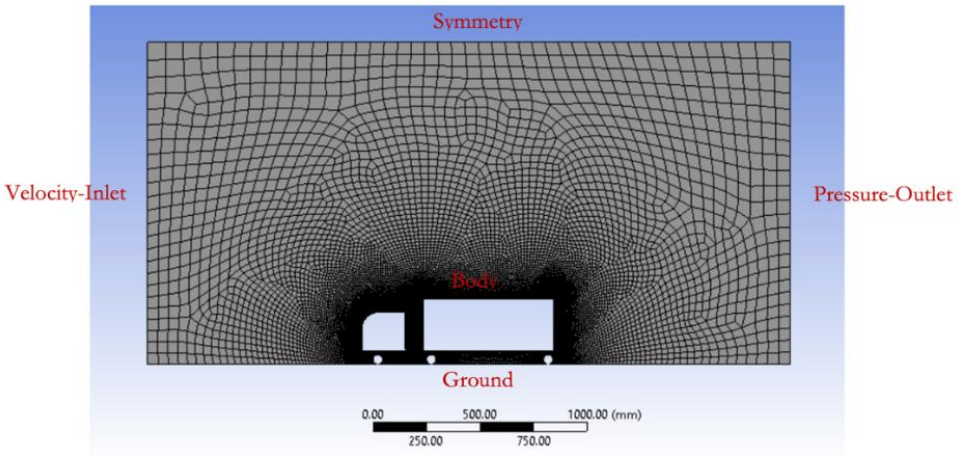

Figure 4: Finished meshed model

In the meantime, the essential mesh metrics with regards to its skewness and orthogonal quality are tabulated in Table 3. The average skewness quality of the mesh metrics is found as 0.18227 whereas the average orthogonal quality is 0.95941. In general, highly skewed cells might make the solution unstable and impede the accuracy of the results. On the whole, these metrics for the skewness and orthogonal quality obtained can be taken to be excellent as indicated by the standard quality spectrum in Ref. [20].

Table 3: Skewness and orthogonal quality mesh metrics

Mesh Metrics	Skewness	Orthogonal Quality
Minimum	0.00106	0.42732
Maximum	0.68227	1.00000
Average	0.18227	0.95941
Standard Deviation	0.10919	0.04560

2.2. Solver

Before conducting the computational analysis, the capability of the CFD solver must be equipped with the pertinent settings for the desired condition. In this case of a rotating cylinder, the velocity and also the position of the cylinder change over time, so a transient analysis is needed to accurately capture the behaviour of the system. With this in mind, a pressure-based transient-state solution is applied for this analysis. The time step size should be small enough to capture the rapid changes in the system but not too small such that the simulation becomes computationally expensive or numerically unstable. The required number of time steps depends on the duration of the simulation and the size of the time step. Table 4 shows the list of the problem-solving techniques and input data.

Calculations are performed on computers utilizing an iterative process where the precision of the result increases with each iteration. In general, k-epsilon (k-ε) model is one of the most common mean flow characteristics for turbulent flow conditions in ANSYS computation, which belongs to Reynolds Averaged Navier-Stokes (RANS) family of turbulence models. The model solves two equations: one for the turbulent kinetic energy, k and another for the rate of dissipation of turbulence, ε. These equations allow for the prediction of turbulence characteristics of the flow field. In this two-equation model, the turbulent characteristics of the flow are represented by two additional transport equations. As a result, a two-equation model may take historical influences like convection and turbulent energy diffusion into consideration. Several previous studies have used k-ε model to simulate the aerodynamics of heavy road vehicles similar to the container lorry in this study. For example, k-ε model was used in a study to analyse

aerodynamic characteristics of a heavy-duty truck [14]. In that study, it has been found that the primary methods for enhancing aerodynamic properties of heavy-duty commercial trucks are by using *k-ε* model and reducing the vortex at the cab and container as well as at the container's end and bottom.

Table 4: The solver setting for this study

General	
Type	Pressure Based
Velocity Formation	Absolute
Time	Transient
2D Space	Planar
Time Step Size	0.01
Number of Time Steps	100
Model	
Viscous	Realizable *k-ε*
Wall Functions	Non-equilibrium
Reference Values	
Velocity	0 – 32 m/s
Cylinder Rotation	1) 0 RPM (static) 2) 3000 RPM or 314.159265 rad/s (rotating)
Reference Area	0.24 m × 0.89 m = 0.214 m^2
2D Space	Planar

There are three versions of the *k-ε* model, which are the standard, Re-Normalisation Group (RNG) and realizable *k-ε* models. The turbulence kinetic energy and dissipation rate equation for these standard, RNG and realizable *k-ε* models are presented by the following equations. Firstly, both Equation 1 and Equation 2 are the transport equations for the standard *k-ε* model.

$$\frac{\partial}{\partial t}(\rho k) + \frac{\partial}{\partial x_i}(\rho k u_i) = \frac{\partial}{\partial x_j}\left[\left(\mu + \frac{\mu_t}{\sigma_k}\right)\frac{\partial k}{\partial x_j}\right] + G_k + G_b - \rho\epsilon - Y_M + S_k \tag{1}$$

$$\frac{\partial}{\partial t}(\rho\epsilon) + \frac{\partial}{\partial x_i}(\rho\epsilon \mathrm{u_i}) = \frac{\partial}{\partial x_j}\left[\left(\mu + \frac{\mu_t}{\sigma_\epsilon}\right)\frac{\partial \epsilon}{\partial x_j}\right] + C_{1\epsilon}\frac{\epsilon}{k}(G_k + \mathrm{C_{3\epsilon}G_b}) - C_{2\epsilon}\rho\frac{\epsilon^2}{k} + S_\epsilon \tag{2}$$

On the other hand, both Equation 3 and Equation 4 are the transport equations for the RNG *k-ε* model.

$$\frac{\partial}{\partial t}(\rho k) + \frac{\partial}{\partial x_i}(\rho k u_i) = \frac{\partial}{\partial x_j}\left[\mathrm{\alpha_k}\mu_{eff}\frac{\partial k}{\partial x_j}\right] + G_k + G_b - \rho\epsilon - Y_M + S_k \tag{3}$$

$$\frac{\partial}{\partial t}(\rho\epsilon) + \frac{\partial}{\partial x_i}(\rho\epsilon \mathrm{u_i}) = \frac{\partial}{\partial x_j}\left[\mathrm{\alpha_\epsilon}\mu_{eff}\frac{\partial \epsilon}{\partial x_j}\right] + C_{1\epsilon}\frac{\epsilon}{k}(G_k + \mathrm{C_{3\epsilon}G_b}) - C_{2\epsilon}\rho\frac{\epsilon^2}{k} - \mathrm{R_\epsilon} + S_\epsilon \tag{4}$$

Finally, both Equation 5 and Equation 6 are the transport equations for the realizable *k-ε* model.

$$\frac{\partial}{\partial t}(\rho k) + \frac{\partial}{\partial x_j}(\rho k u_j) = \frac{\partial}{\partial x_j}\left[\left(\mu + \frac{\mu_t}{\sigma_k}\right)\frac{\partial k}{\partial x_j}\right] + G_k + G_b - \rho\epsilon - Y_M + S_k \tag{5}$$

$$\frac{\partial}{\partial t}(\rho\epsilon) + \frac{\partial}{\partial x_j}(\rho\epsilon \mathrm{u_j}) = \frac{\partial}{\partial x_j}\left[\left(\mu + \frac{\mu_t}{\sigma_\epsilon}\right)\frac{\partial \epsilon}{\partial x_j}\right] + \rho\mathrm{C_1}S\epsilon - \rho C_2\frac{\epsilon^2}{k + \sqrt{v\epsilon}} + \mathrm{C_{1\epsilon}}\frac{\epsilon}{k}\mathrm{C_{3\epsilon}G_b} + S_\epsilon \tag{6}$$

In the above equations, G_k stands for the creation of turbulence kinetic energy owing to the mean velocity gradients while G_b is the generation of turbulence kinetic energy due to buoyancy. Furthermore, Y_M is the variable dilatation in compressible turbulence's contribution to total dissipation rate, α_k is the inverse effective Prandtl number for k, α_ε is the inverse effective Prandtl number for ε, σ_k is turbulent Prandtl value for k, σ_ε is turbulent Prandtl value for ε, ϱ is fluid density, u is fluid velocity, x_i and x_j are the Cartesian coordinate direction, ε is turbulence dissipation rate, μ is the fluid dynamic viscosity, and μ_t is the turbulent viscosity. Last but not the least, $C_{1\varepsilon}$, C_2, $C_{2\varepsilon}$ and $C_{3\varepsilon}$ are constants while S_k and S_ε are user-defined source terms.

Generally, the k-ε turbulence model might not be effective in predicting turbulence flow in certain situations, particularly when there are unfavourable pressure gradients present. This is mainly because the k-ε model assumes that the turbulent stresses are proportional to the mean flow gradient, which may not be accurate in cases where the pressure gradient is high [21]. Researchers have shown that in cases of strong adverse pressure gradients, k-ε model can lead to erroneous predictions and may not accurately capture the flow behaviour [22]. It can be noted that the RNG k-ε model is the modified version of the standard k-ε model, which includes added model constants and terms to further improve the accuracy of the predictions. Meanwhile, the k equation for the realizable k-ε model is similar to the standard k-ε model with the added constants but the ε equation is notably different between the two k-ε models. As can be observed in Equation 6, it is interesting to note that it does not have the same G_k term as other k-ε models as it does not involve the production of k. In essence, this current form is thought to depict the transmission of spectral energy more accurately. The destruction term, which is the last term on the right side of Equation 6, does not have any singularities and this indicates that even if k disappears or shrinks to zero, its denominator will never do. This is a much desirable feature and stands in contrast to conventional k-ε models, which exhibit a singularity because k is present in the denominator. Due to this feature, realizable k-ε model is used to overcome the well-known shortcomings of the conventional k-ε model. With the use of this model, it is feasible to obtain satisfactory results for integral values such as the drag coefficient that are more accurate, converge rapidly and quite stable.

2.3. Validation study for solver accuracy

To evaluate the accuracy of the findings produced by using the aforementioned solver parameters, initial test case of the baseline container lorry design model without any rotating cylinder is conducted. The simulated relative inlet airspeed for this test case is between 0 m/s to 31.5 m/s. The results obtained from the simulation analysis are compared with the published experimental results in Ref. [15], which is shown in Figure 5. It can be observed that the drag coefficient, C_d obtained from the simulation analysis is closely similar to the one obtained from the wind tunnel experiment. The value difference is less than 10%, which is taken to be within acceptable range of accuracy for Reynolds number, Re ranging between 0 to 600,000. All in all, the solver parameters are taken to be appropriate to be for this analysis study.

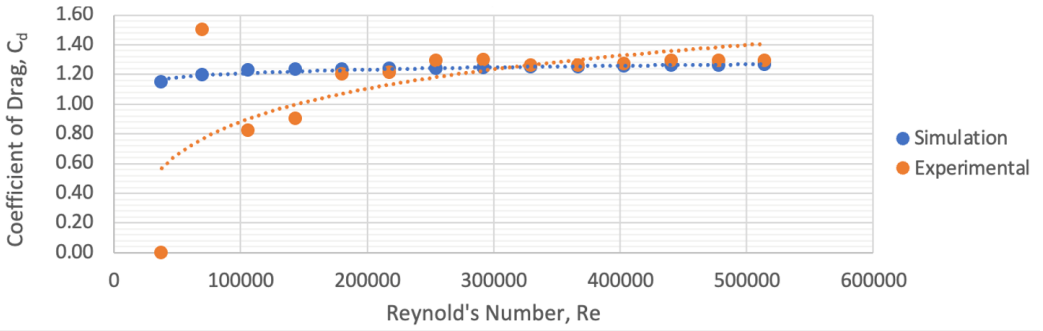

Figure 5: C_d vs Re obtained from the validation study

3. Results and Discussion

There are three control variables that are varied in the CFD simulation analysis for this study. The first one is the velocity of the air entering the inlet, which is varied between 0 m/s to 32 m/s to control and manipulate Re around the airflow of the truck. The second variable is the rotation of the cylinder, where is set for two conditions: static and moving (rotating). The rotational speed of the cylinders is set to 3000 RPM for the simulated moving condition. Finally, the last variable is the position of the cylinder as indicated in previous Figure 2.

3.1. Comparison with experimental results for three initial positions of the cylinder

The results of previous validation study in Figure 5 are taken as the baseline reference. To compare with the previous experimental results as published in Ref. [15], the simulation analysis is conducted for the three initial positions of the rotating cylinder as illustrated in previous Figure 2. Figure 6 shows the previous experimental results while Figure 7 depicts the results of CFD simulation analysis in this study.

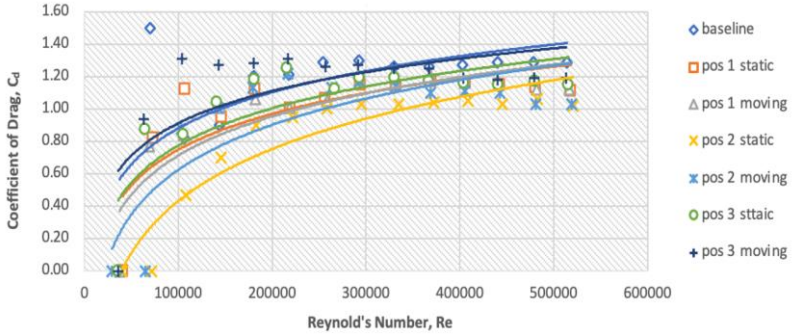

Figure 6: Experimental results of C_d vs Re for three initial positioning

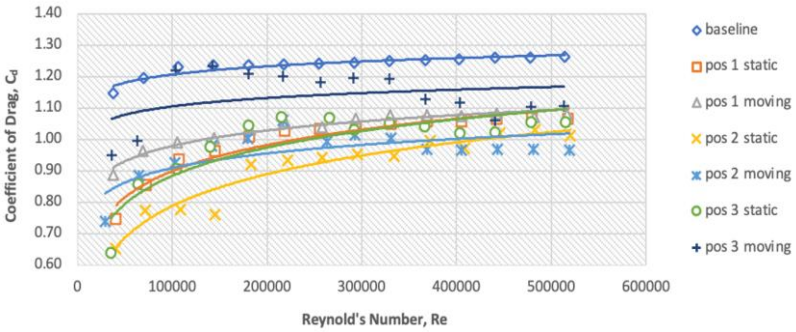

Figure 7: Simulation results of C_d vs Re for three initial positioning

For the first positioning of rotating cylinder, it can be observed that simulation result is more stable and steadier with increasing Re in comparison to experimental data where it fluctuates back and forth in the first few takes before becoming more stable toward higher Re. Average differences of 7.05% and 7.85% are respectively recorded between the results of the simulation and the experiment for static and moving conditions at this first initial position. It can be observed that the static cylinder performed more efficiently as compared to the moving cylinder, which is reflected by the lower average C_d for the static cylinder than that of the moving cylinder. Nonetheless, note that this difference is just significant at low Re and as Re increases, the values of C_d converges to around the same values for both static and moving cylinder conditions. This observation trend is true for both simulation and experimental results. Similar observation can also be seen for the second initial positioning of the cylinders. In this case, the average

differences between the simulation and the experimental results are 9.70% and 9.89% for the static and moving configurations of the cylinders, respectively. The results from simulation analysis are more stable and steadier. Moreover, at this positioning, the static cylinder has again performed more effectively than the moving cylinder. The noted differences between them are significantly visible at low Re but diminish as Re increases. On the other hand, for the third considered initial positioning of the cylinder, average differences between simulation and experimental results for both static and moving configurations of the cylinders are 9.68% and 6.70%, respectively. Based on previous Figure 6 and Figure 7, it is noticeable that values of C_d for both static and moving cylinder configurations increase at low Re up until it reaches 200,000 where it began to slowly decrease. For Re higher than 200,000, C_d has minor fluctuations and inconsistencies, and shows a visible trend between the static and moving cylinder configurations. Static cylinder configuration is shown to achieve a much better drag reduction than the moving configuration. This could be attributed to the RPM incompatibility with relative free stream velocity that has caused more turbulence in the air and affected the drag of the container lorry.

Overall, for these three initial considered positioning of the rotating cylinder, both simulation and experimental results show that the static second position corresponds to the lowest value of C_d, which is about 25.50% reduction compared to the other considered configurations. It is also good to note that the moving cylinder configuration at each position has higher drag compared to the static configuration. This could be because the chosen RPM is not optimal for velocity of free stream air and positioning of the cylinder used in this study. Nonetheless, the moving cylinder configurations still perform better than the baseline container lorry model

3.2. Simulation results for three new positions of the cylinder

Figure 8 shows the simulation results for the first new considered positioning of rotating cylinder on the container lorry model. It can be observed, unlike the result for previous initial positioning of the cylinder, the trend of C_d appears to bend downward. As Re increases, the value of C_d for both static and moving cylinder configurations significantly reduces up until Re of 300,000. Although the static cylinder configuration initially performs better than the moving cylinder configuration, its corresponding value of C_d starts to increase and ultimately converge with that of the moving cylinder configuration when Re is above 300,000. All in all, implementation of the static and moving rotating cylinder is shown to reduce the C_d of the container lorry by averagely 18.74% and 18.5%, respectively.

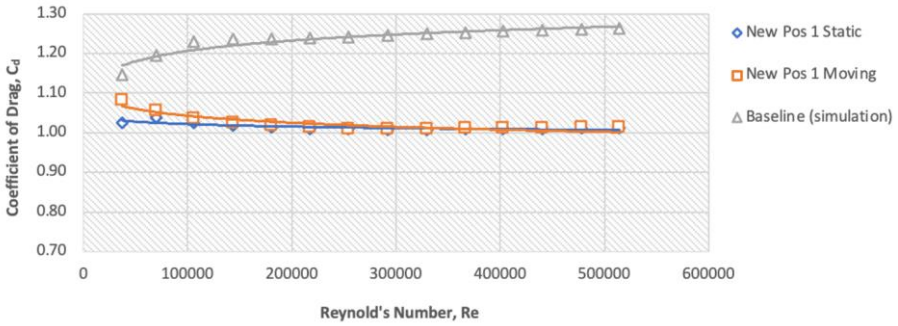

Figure 8: Simulation results of C_d vs Re for first new position

A similar trend is also essentially observed for the second new positioning of the rotating cylinder as depicted in Figure 9. Values of C_d for both static and moving cylinder configurations decrease with increasing Re up until about 300,000. After that point, values of C_d seem to have converged and maintain at the same value with increasing Re. In similar fashion, despite drag performance of the static cylinder configuration is better at lower Re, the values of C_d for both static and moving cylinder configurations

ultimately converge to a similar value at high Re. In terms of comparison with the drag performance for the baseline container lorry, implementing the static and moving cylinder configurations can reduce the value of C_d by 36.0% and 35.8% on average, respectively. As presented in Figure 10, an essentially similar trend to Figure 9 is observed for the drag performance of the static and moving cylinder configurations at the third new positioning. At this considered new third position, average drag reduction of 26.2% and 25.7% has been obtained by implementing the static and moving cylinder configurations, respectively, as compared to that for the baseline container lorry design model.

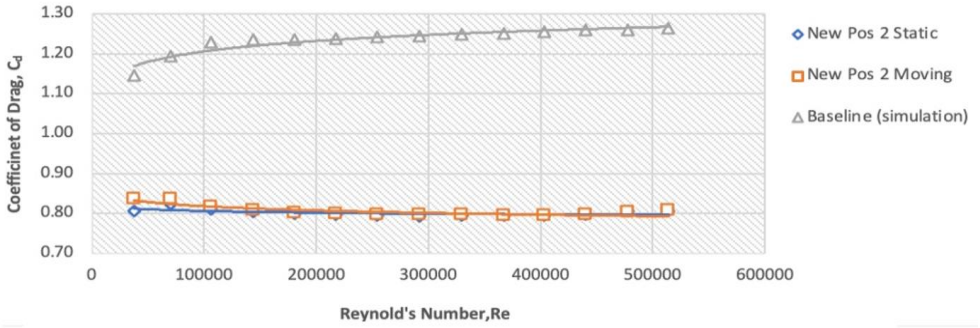

Figure 9: Simulation results of C_d vs Re for second new position

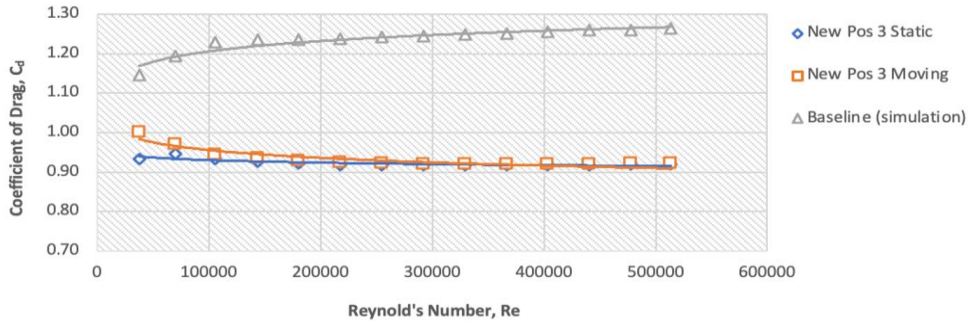

Figure 10: Simulation results of C_d vs Re for third new position

On the whole, it is clearly seen from the obtained simulation results that the new second positioning of the rotating cylinder has the best drag performance. This can be contributed to the reduction of the drag on the container lorry as it helps to diminish the turbulence that is created when the vehicle moves. At the rear of the container lorry, with this placement of the rotating cylinder, it will disrupt and disperse the air around it, which reduces the created air turbulence and subsequently lessens the drag. Figure 11 illustrates the velocity streamlines where recirculation or swirling of airflow at the rear of the container lorry by placing the rotating cylinder at the considered new second position. It should also be noted that this positioning of rotating cylinder on the container lorry performs much better than any of the three initial positions discussed in previous section.

Moreover, the observed independence of C_d towards Re beyond the certain limit is believed to be likely due to the formation of a fully turbulent boundary layer over the surface of the object, which leads to relatively constant level of skin friction drag. This notion is supported by several previous researches. For instance, a study found that C_d of a sphere became independent of Re when it reached the critical Re value of 3.5×10^5, which corresponds to the condition for the onset of fully turbulent boundary layer flow [23]. In this case, the transition from laminar to turbulent in the boundary layer around the sphere is what causes the higher momentum at the boundary and the delay in the flow separation [24]. It should be noted that the value of Re at which the C_d becomes independent may depend on various factors such

as the shape and surface roughness of the object, as well as the flow conditions. Further research needs to be conducted to investigate the exact mechanism behind this phenomenon and determine the specific conditions in which it will occur for different objects.

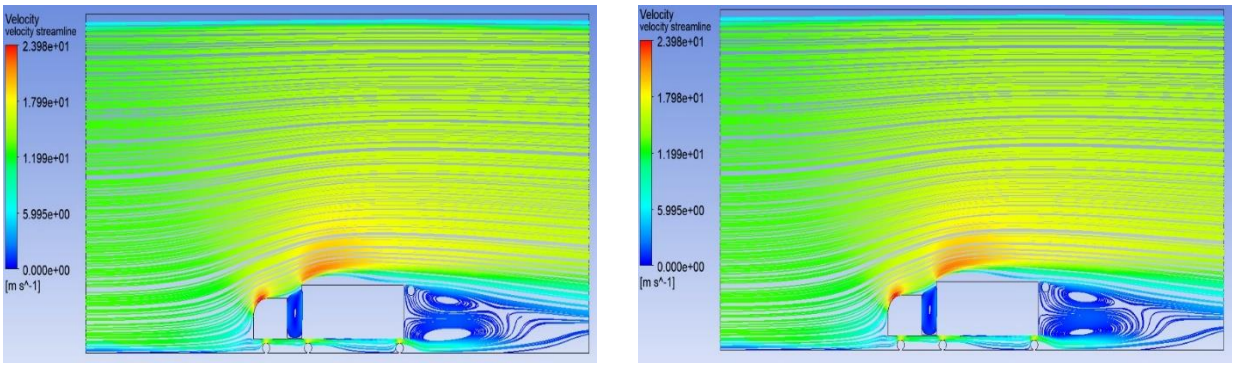

(a) Static cylinder configuration (b) Moving cylinder configuration

Figure 11: Velocity streamlines of container lorry with new second positioning of rotating cylinder

4. Conclusion

This research work explores the possible effects of using rotating cylinder as drag reducers on the container lorry design. In total, six different positions of the rotating cylinder on the container lorry are considered, with two modes of static and moving configurations at each position. The CFD simulation analysis is carried out for this study using the ANSYS software. All in all, based on the results, it can be concluded that the use of rotating cylinder has a good potential to reduce the drag on the container lorry when it moves on the road. Of all the six considered positioning, the new second position of the rotating cylinder is shown to have the best drag performance, which corresponds to about 36.0% reduction in drag compared to that of the clean baseline design of the container lorry without any rotating cylinder. In addition, the static cylinder configuration outperforms the moving cylinder configuration at each of the considered positions. This situation can be contributed to the less than ideal setting of the RPM for the moving cylinder with respect to the settings of free-stream air velocity and cylinder location. For the future work, the design of the rotating cylinder can be enhanced. In this simulation study, the cylinder is designed as a plain cylinder shape. Various other cylinder designs can be explored to study the effects of its shape on the drag performance of the heavy road vehicles. Furthermore, the analysis on the cost-efficiency of implementing this drag reducing mechanism can also be done.

Acknowledgement

The authors acknowledge the funding of this research from Ministry of Education Malaysia through their Fundamental Research Grant Scheme: FRGS/1/2018/TK09/UPM/02/2 (Project Code: 03-01-18-1950FR).

References

[1] R. McCallen, R. Couch, J. Hsu, F. Browand, M. Hammache, A. Leonard, M. Brady, K. Salari, W. Rutledge, J. Ross, B. Storms, J. T. Heineck, D. Driver, J. Bell, and G. Zilliac, 'Progress in Reducing Aerodynamic Drag for Higher Efficiency of Heavy Duty Trucks (Class 7-8)', SAE Technical Paper Series, 1999-01-2238, 1999.

[2] S. Balkanyi, L. Bernal, B. Khalighi, and V. Sumantran, 'Dynamics of Manipulated Bluff Body Wakes', Fluids 2000 Conference and Exhibit, Denver, USA, 19-22 June, 2000.

[3] H. Chowdhury, H. Moria, A. Ali, I. Khan, F. Alam, and S. Watkins, 'A Study on Aerodynamic Drag of a Semi-Trailer Truck', Procedia Engineering, vol. 56, pp. 201-205, 2013.
[4] R. Snyder, 'Tire Rolling Losses and Fuel Economy', SAE Special Publication, 74, 1997.
[5] H. Chowdhury, B. Loganathan, I. Mustary, H. Moria, and F. Alam, 'Effect of Various Deflectors on Drag Reduction for Trucks', Energy Procedia, vol. 110, pp. 561-566, 2017.
[6] D. Landman, R. Wood, and W. Seay, 'Understanding Practical Heavy Truck Drag Reduction Limits', SAE Publication, 2009-01-2890, 2009.
[7] R. E. Schoon, 'On-road Evaluation of Devices to Reduce Heavy Truck Aerodynamic Drag', SAE Technical Paper, 0148-7191, 2007.
[8] J. Christensen, K. P. Glaeser, T. Shelton, B. Moore, and L. Aarts, "Innovation in Truck Technologies," OECD/ITF Joint Transport Research Centre Discussion Paper, 2010.
[9] M. F. Sari, 'The Aerodynamic Analysis of Air Resistance Affecting the Front Form of Light Commercial Vehicles and Its Effect on Fuel Consumption', Master Thesis, Osmangazi University, Turkiye, 2007.
[10] S. K. Meredith, M. Kosseifi, and J. Pastore, 'Airflow Baffle for Commercial Truck Fuel Efficiency Improvements', U.S. Patent Appl. 13/715,004, 2014.
[11] V. Modi, S. S. Hill, and T. Yokomizo, 'Drag Reduction of Trucks Through Boundary-Layer Control', Journal of Wind Engineering and Industrial Aerodynamics, vol. 54, pp. 583-594, 1995.
[12] P. Gilliéron, and A. Kourta, 'Aerodynamic Drag Reduction by Vertical Splitter Plates', Experiments in Fluids, vol. 48, no. 1, pp. 1-16, 2010.
[13] G. Fourrié, L. Keirsbulck, L. Labraga, and P. Gilliéron, 'Bluff-Body Drag Reduction Using a Deflector', Experiments in Fluids, vol. 50, pp. 385-395, 2011.
[14] B. Ying, 'Boundary-layer Control of Bluff Bodies with Application to Drag Reduction of Tractor-trailer Truck Configurations," Master Thesis, University of British Columbia, Canada, 1991.
[15] A. S. Hamdan, 'Experimental Investigation on Static and Spinning Cylinder and Its Positioning as a Drag Reducer on Truck's Container', Bachelor Thesis, Universiti Putra Malaysia, Malaysia, 2022.
[16] H. M. Ali, A. S. M. Rafie, and S. A. M. Ali, 'Numerical Analysis of Leading Edge Cylinder Aerofoil on Selig S1223 for Moving Surface Boundary Control', Journal of Aeronautics, Astronautics and Aviation, vol. 53, no. 2, pp. 143-154, 2021.
[17] H. M. Ali, A. S. M. Rafie, S. A. M. Ali, and E. Gires, 'Computational Analysis of the Rotating Cylinder Embedment onto Flat Plate', CFD Letters, vol. 13, no. 12, pp. 133-149, 2021.
[18] H. M. Ali, A. S. M. Rafie, M. F. A. Hamid, and S. A. M. Ali, 'Comparative Computational Study of Double Rotating Cylinder Embedded on Selig S1223 Aerofoil and Flat Plate for High Altitude Platform', Pertanika Journal of Science and Technology, vol. 30, no. 4, pp. 2767-2788, 2022.
[19] M. Arafat, I. A. Ishak, and A. F. Mohammad, 'Influence of Mesh Refinement on the Accuracy of Numerical Result for the Next-Generation High-Speed Train Aerodynamics', OSF Preprints, 2023.
[20] N. Fatchurrohman, and S. Chia, 'Performance of Hybrid Nano-Micro Reinforced Mg Metal Matrix Composites Brake Calliper: Simulation Approach', IOP Conference Series: Materials Science and Engineering, vol. 257, 012060, 2017.
[21] B. E. Launder, and D. B. Spalding, 'The Numerical Computation of Turbulent Flows', Computer Methods in Applied Mechanics and Engineering, vol. 3, pp. 269-289, 1974.
[22] P. Spalart, and S. Allmaras, 'A One-Equation Turbulence Model for Aerodynamic Flows', 30th Aerospace Sciences Meeting and Exhibit, Reno, USA, 6-9 January, 1992.
[23] N. Moradian, D. S. Ting, and S. Cheng, 'Advancing Drag Crisis of a Sphere via the Manipulation of Integral Length Scale', Wind and Structures, vol. 14, no. 1, p. 35, 2011.
[24] J. M. Cimbala, and Y. A. Cengel, 'Fluid Mechanics: Fundamentals and Applications', McGraw-Hill, 2006.